Consolidated Chemical Provinces on Mars

A. Rani, A. Basu Sarbadhikari, D. Hood, O. Gasnault, S. Nambiar, S. Karunatillake

Consolidated Chemical Provinces on Mars: Implications for Geologic Interpretations

A. Rani[1,2], A. Basu Sarbadhikari[1,*], D. R. Hood[3], O. Gasnault[4], S. Nambiar[1] and S. Karunatillake[5]

[1]Physical Research Laboratory, Planetary Sciences Division, Ahmedabad, Gujarat 380009, India

[2]Indian Institute of Technology, Gandhinagar, Earth Sciences, Gujarat 382355, India

[3]Baylor University, Department of Geosciences, Waco, Texas 76798, USA

[4]Institut de Recherche en Astrophysique et Planétologie, Université de Toulouse, CNRS, CNES, 31028 Toulouse, France

[5]Louisiana State University, Geology and Geophysics, Baton Rouge, Louisiana 70808, USA

***Correspondence to:** A. Basu Sarbadhikari, amitbs@prl.res.in

Key Points:

- We have consolidated three key multivariate methods, yielding the first unified set of chemical provinces of Mars
- Igneous geochemistry pervades volatile-rich regions, consistent with water-limited isochemical weathering throughout Mars's geologic history
- Secular chemical trends suggest complex processes of mantle melting for highlands, which differs from a possibly garnet-rich lowland source

Abstract

Chemical provinces were defined on Mars a decade ago using orbital nuclear spectroscopy of K, Th, Fe, Si, Ca, Cl, and H_2O. However, past multivariate analyses yielded three sets of provinces, suggesting methodologic variability. Province-stability to the inclusion of Al and S is also unknown, presenting additional uncertainties for geologic insight. Here we consolidate key multivariate methods to define the first cross-validated provinces. In southern highlands, the highly incompatible K and Th show non-uniform distribution with higher values in mid Noachian and Hesperian than late Noachian – early Hesperian volcanic terrains. Silica- and Al-depletion trends from Noachian to Amazonian indicate highly differentiated mantle with variable degree of melting. Late Hesperian lowlands are highly depleted in Al and enriched in K and Th, consistent with volcanic resurfacing from a low-degree partially melted, garnet-rich mantle. Furthermore, older volatile-rich regions such as Medusae Fossae Formation exhibit igneous geochemistry, consistent with water-limited isochemical weathering throughout Mars's history.

Plain Language Summary

Topographically Mars can be divided into two large regions: southern highlands and northern lowlands. However, the compositional evolution of these two landforms and their source characteristics remains unclear. Therefore, using enhanced satellite nuclear spectroscopic data, we develop a set of consolidated geochemical provinces of Mars using three multivariate analysis techniques. We identified the correlation of distinct geochemical provinces with mapped geologic units, which demonstrates the effect of bedrock composition over bulk soil composition. Our study depicts discrete igneous provinces within the southern highlands, which follow a secular chemical pattern, indicating a highly differentiated mantle

54 source with an evolving formation pressure and degree of melting. The northern lowlands, on
55 the other hand, are uncorrelated with the chemical trend of southern highland provinces,
56 suggesting a distinct evolution. Our findings further reveal that regardless of volatile
57 enrichment, igneous crustal composition dominates over chemical alteration signatures
58 indicating a limited role of liquid water on the martian landscape.

59

60 **1. Introduction**

61 A *trilogy* of multivariate cluster analysis methods applied to the chemical maps
62 derived from Mars Odyssey gamma-ray and neutron spectroscopy (GRS) initially identified
63 chemical provinces and supported interpretations of regional-scale geology (Karunatillake et
64 al., 2009; Gasnault et al., 2010; Taylor et al., 2010). However, the lack of an inter-
65 methodological synthesis to characterize geological processes has hindered subsequent works
66 and stymied advances with other datasets (cf., Rogers & Hamilton 2015). Furthermore, key
67 chemical maps used in subsequent papers (Baratoux et al., 2014; Ojha et al., 2018; Plesa et
68 al., 2018) were unavailable or only in a preliminary state for the original trilogy: Aluminium
69 (Al), sensitive to both igneous evolution and secondary mineralogy (cf., Nimmo & Tanaka,
70 2005; Ehlmann et al., 2011; McLennan, 2012); and Sulfur (S), sensitive to cycling processes
71 within the martian critical zone across the atmosphere and crust (Halevy et al., 2007; King &
72 McLennan, 2010).

73 Here we use nine elemental mass fraction maps from the GRS: key rock-forming
74 elements (Fe, Si, Ca, and Al) with large ion lithophiles (K and Th) and volatiles
75 (stoichiometrically equivalent H_2O, Cl, and S) to resolve the aforementioned challenges. We
76 synthesize and advance prior multivariate methods (Karunatillake et al., 2009; Gasnault et al.,
77 2010; Taylor et al., 2010) to derive the first consolidated chemical provinces of Mars. We

consider three of the provinces as case studies on geologic insight, revealing diverse mantle sources and magmatic processes in volcanic areas, characterizing possible global ashfall units, and evaluating the relative roles of igneous versus aqueous environments.

2. Data and Methods

We use chemical maps derived from GRS spectra to delineate the chemically distinct provinces. The average decimetre sampling depth and coarse spatial resolution of GRS overcome the effects of fine dust mantles making GRS elemental analysis ideal for primary and secondary geological process studies on broad scales. GRS measures the energy spectrum of gamma photons emitted from the martian surface and characteristic spectral peaks allow us to measure the abundance and distribution of most major rock-forming elements, along with some minor elements present on the martian surface. There are two main processes on the martian surface that give rise to gamma-photon emission. Gamma photons can be emitted from the decay of natural radioactive elements (K and Th) or emissions induced by cosmic particle interactions with the martian atmosphere and non-radioactive elements of the martian surface. However, due to increasing H (reported as stoichiometric H_2O mass fractions) towards the poles causing mass dilution for radioactive elements and compositional modelling issues for others due to neutron moderation, derived chemical maps are restricted to the mid-to-low latitudes, roughly within $\pm 50^{o}$. Furthermore, chemical maps are generated at a resolution of $5^{o} \times 5^{o}$ due to broad footprint of the GRS instrument (Boynton et al., 2007). We use the latest refined datasets of GRS, including Al and S used in the literature (cf., Hood et al., 2016, 2019; Ojha et al., 2018, 2021), and compare them with GRS data used a decade ago (Boynton et al., 2007; Karunatillake et al., 2009; Gasnault et al., 2010; Taylor et al., 2010), including the archived data at the NASA

Planetary Database System (https://pds-geosciences.wustl.edu/ody/ody-m-grs-5-elements v1/odgm_xxxx/data/smoothed/). The delineation of provinces also mitigates the substantial spatial autocorrelation inherent in the GRS data by associating large chemical deviations with multi-pixel regions rather which are larger than the GRS instrument footprint (Karunatillake et al., 2009). The detailed description and comparison of old versus latest refined datasets of GRS are described in Supplementary Information S1.

2.1. Multivariate Cluster Analysis

We apply three multivariate cluster analyses to discern a set of internally uniform chemical provinces that reflect the compositional variability of the martian crust. The three methods (**Supporting Information S1.2** provides more details) consist of non-hierarchical clustering with principal component analysis (NHC-PCA: Taylor et al., 2010), hierarchical clustering with principal component analysis (HC-PCA: Gasnault et al., 2010), and modified student's t-test to distinguish spatially overlapping Gaussian tail clusters (t-GTC: Karunatillake et al., 2009).

The three methods optimize clustering differently but still present spatially overlapping trends suggestive of distinct provinces. NHC-PCA optimizes Euclidian distances between cluster centers, where the number of clusters is specified a priori. In comparison, HC-PCA builds a hierarchy of clusters using a top-down clustering approach based on a divisive algorithm (Kaufman & Rousseeuw, 2005), where the complete martian landscape mapped by GRS belongs to one cluster and is split iteratively, moving down the hierarchy to highlight the differences between the sub-clusters. The modified t-GTC method identifies spatially contiguous areas where two or more elements deviate from their respective average mid-to-low latitude crustal abundances by one standard deviation or greater. The t-GTCs and

HC-PCA-derived provinces reduce spatial autocorrelation biases by using unclassified (boundary) pixels to separate provinces from each other. Complementarily, the NHC-PCA method delineates border-sharing provinces.

We combine the intermediate provinces from the NHC-PCA, HC-PCA, and t-GTC methods into a consolidated map using a spatial contouring approach. A contour map of provinces is made by categorizing the regions into three levels: provinces derived from all three-methods overlapping, provinces with any two-methods overlapping, and provinces with no overlap (**Figure S1**). We demarcate the boundaries of final provinces resulting from at least two-methods overlapping, reducing the spatial uncertainty in any method (**Supporting Information S2** provides more details). Provinces that deviate minimally from the average martian crust (AMC) composition (**Supporting Information S2.1** and **S2.2**) are omitted so that the consolidated chemical province map highlights crustally distinct regions. In addition, we use mapped geology (Tanaka et al., 2014) for context on chemical trends.

3. Results

All three methods lead to large chemically uniform provinces, with minimal intra-province compositional variance, reinforcing the subdued variability in chemical maps of Mars. The intermediate chemical province sets resulting from the three underlying methods (**Supporting Information S2** provides more details**)** are labeled numerically (Province-1 to Province-6; **Figures 1a-c** and **Tables S1** and **S2**). Province-2 from NHC-PCA and HC-PCA methods lacks the minimum criterion of at least two methods overlapping (**Figure S1; Supporting Information S2** provides more details), and Province-4 is compositionally identical to the AMC within statistical uncertainty. Therefore, Province-2 and 4 are de-prioritized in the consolidated chemical province map (**Figure 1d**). Moreover, provinces that

overlap spatially across the methods are compositionally similar even if driven by different multivariate methods (**Tables S2, S3**). This further justifies our contour-consolidation method yielding the merged chemical province map (**Figure 1** and **Tables 1** and **S3).** Overall, overlapping areas labeled as 'Province-1' in **Figures 1a-c** have been combined into 'Province-A', 'Province-3' into 'Province-B', 'Province-5' into 'Province-C', and 'Province-6' into 'Province-D', resulting in four consolidated provinces (**Figure 1d** and **Tables 1** and **S1**). Compositional consistency across the numeric intermediate provinces enables this synthesis (**Supporting Information S2**). While geographically widely separated areas may constitute a single province, such regions show some compositional heterogeneity.

3.1. Distinct Geochemical Provinces

Four geographically distributed regions in the southern highlands constitute Province-A (**Figure 1d**). This province broadly represents mid and late Noachian highlands (> 30%) to early Hesperian aged volcanic units (> 20%) (**Figures 2a** and **S2**), containing many of the large Hesperian volcanic provinces. This province is enriched in Al and depleted in K, Th, and volatiles (H_2O, S, Cl) relative to the AMC (**Figure 2b** and **Tables 1, S3,** and **S4; Supporting Information S2.2**). The K/Th and S/Cl ratios are above average, while the Fe/Si ratio is consistent with the AMC.

Province-B comprises Amazonian and Amazonian-Hesperian aged volcanic units (> 30%) with Amazonian to Hesperian transitional geological units (~ 18%) (**Figures 2a** and **S2**). The distribution of K and Th is consistent with the AMC (Taylor et al., 2006); however, the K/Th ratio is slightly low compared to the AMC (**Figure 2b** and **Tables 1, S3** and **S4; Supporting Information S2.2**). This province is moderately depleted in Si, Ca, and Fe and highly depleted in Al, while the volatiles (especially Cl and S) are highly enriched relative to

174 the AMC. The S/Cl ratio is depleted from preferential Cl enrichment. Compared to the AMC,
175 the Fe/Si ratio is below average.

176 Province-C consists of two geographic regions: Sinus Meridiani (SM) and the
177 Medusae Fossae Formation (MFF), dominated by mid-Noachian highlands (~ 40 %) (**Figures**
178 **1d, 2a,** and **S2** and **Table S1**). These regions are enriched in volatiles (H_2O, Cl, and S) (cf.
179 Diez et al. 2008; Feldman et al., 2011; Maurice et al., 2011), while Fe, Ca are slightly
180 enriched relative to the AMC (**Figure 2b** and **Tables 1, S3** and **S4; Supporting Information**
181 **S2.2**). The ratio of S/Cl and K/Th is consistent with the AMC. However, Fe enrichments
182 make the Fe/Si ratio higher relative to the AMC.

183 Two regions of broadly late Hesperian lowlands form Province-D (> 60%) (**Figures**
184 **2a** and **S2**). It is confined to Southern Acidalia Planitia and Utopia Planitia of the Northern
185 lowland near the dichotomy boundary (**Figure 1d** and **Table S1**). Since both these regions
186 are found within the northern lowlands and the northern extent of each is obscured by the
187 chemical mapping boundary (**Supporting Information S1**), they may constitute a larger,
188 contiguous region. The broader extent of Province-D, which includes the western and eastern
189 part of this province, spatially overlaps with the TES-derived Surface Type 2 mineralogy in
190 the martian northern lowlands (Bandfield et al., 2000; Rogers et al., 2007; Rogers &
191 Hamilton 2015). This province is highly depleted in Al, enriched in Si, Fe, K, and Th relative
192 to the AMC (**Figure 2b** and **Tables 1, S3** and **S4**), contrasting with other provinces. The
193 K/Th and S/Cl ratio is consistent with the AMC, whereas Fe/Si is higher.

194

195 **4. Discussion**

196 **4.1. Extent of aqueous alteration and K/Th trends**

197 We first evaluate the extent of aqueous alteration evident at regional scales to
198 decimeter depths. The Chemical Index of Alteration
199 (CIA=$Al_2O_3/(Al_2O_3+CaO+Na_2O+K_2O)\times100$) in standard molar abundances of oxides
200 corresponding to the provinces A-D is < 50, which indicates no signature of weathering
201 (**Figure 2c**) at these broad scales. The K/Th ratio is similar across all the provinces, and with
202 the AMC within statistical uncertainty (**Figure 2b**). Specifically, K/Th ratio is effectively
203 invariant with the abundance of the volatiles (H_2O, SO_3, and Cl) even across the maximum in
204 Province-C to a minimum in Province-A (**Figure 3a**). The most incompatible mapped
205 elements, K and Th (partition coefficient <<1; Borg & Draper, 2003) do not fractionate in the
206 solid phases during magmatic processes. Collectively, our study shows that even the volatile-
207 rich regions are compositionally consistent with water-limited isochemical weathering
208 throughout Mars's geologic history (Hurowitz & McLennan, 2007; Tosca et al., 2008).
209 Consequently, the provinces are broadly representative of well-preserved igneous processes
210 at least to decimeter depth scales and averaged over a few hundred kilometres horizontally.

211

212 **4.2. Secular chemical trends on Mars**

213 Earlier work by Taylor et al. (2010) grouped all volcanic landscapes into a single
214 province irrespective of age. However, our study supports the findings (Karunatillake et al.,
215 2009; Gasnault et al., 2010) that volcanic regions form separate provinces by age (**Figure**
216 **2a**), as shown by Baratoux et al. (2011). Moreover, the minimally weathered secular volcanic
217 composition of provinces A-C in the southern highlands of Mars shows distinct geochemical
218 trends. Unlike southern highlands, Province-D, the late Hesperian lowland unit, deviates from
219 the secular chemical trend (**Figure 3b-d**), indicating distinct lithology. The provinces A-C
220 from mid-Noachian to Amazonian show Al-, Fe-, Si- and Ca-depletion (**Figure 3b-d**). As

hypothesized by Balta & McSween (2013), higher SiO_2 in older regions of Mars may indicate dehydration melting of the mantle with hundreds of mg/kg water, similar to that of Province-A and -C of our study, in contrast to the relatively silica-depleted younger Province-B. Unlike Earth, considering a stagnant-lid regime of Mars (Golombek & Phillips, 2009; Grott et al., 2013), the decrease of SiO_2 and concomitant increase in olivine component in the parent magma from the oldest to youngest volcanic terrains of southern highlands could be explained by the growth of lithospheric thickness, which would increase the formation pressure, supporting the results of Baratoux et al. (2013). This contrasts with the topmost micron-layer observation by Thermal Emission Spectrometer (TES), suggestive of weathering reflected by the non-detection of olivine in the Hesperian highland terrains, at the spatial resolution of 1 pixel per degree (Rogers & Hamilton, 2015). GRS-scale footprints in this study consistently reveal the igneous crustal composition albeit weathering processes was prevalent during martian surface evolution. In addition, high Ca/Al for Province-B and -D could indicate a path for sampling a high-pressure, garnet-rich source (Treiman, 2005; Dasgupta & Hirschmann, 2007; Balta & McSween, 2013). The abundances of K and Th are relatively low in late Noachian – early Hesperian Province-A as compared to Hesperian-Amazonian Province-B and mid-Noachian Province-C in the highland volcanic terrains (**Figure 3e**). Earlier studies advocated the early Noachian crust building phenomenon for the enrichment of these large ion lithophile elements (LILEs: K and Th) in Noachian than Hesperian terrains (Rogers & Hamilton, 2015). However, our study shows that the youngest volcanic province also contains a high relative abundance of those LILEs, which contradicts the hypothesis of LILE fractionation during the early Noachian crust formation. Moreover, the non-systematic trend of the abundances of LILEs and other secular chemical trends may necessitate complex melting processes in a highly differentiated mantle source on a regional

to global scale (cf. Basu Sarbadhikari et al., 2016; 2017; Udry et al., 2020) that existed from the early-stage evolution of Mars.

Compared to prior works, the emergence of distinct regions as well as the exclusion of previously suggested provinces (**Figure 1d**) reflects our methodological advances along with the use of Al and S. Given the collective distinctness among the consolidated chemical provinces, we consider three regions for detailed case studies: Lunae Planum, Medusae Fossae Formation, and Southern Acidalia Planitia (**Figure 1d**).

4.3. Lunae Planum (LP) in Province-A

LP region is a geologically distinct plateau of early Hesperian-aged highland material (Tanaka et al., 2014), which lies between Chryse Planitia and Olympus Mons in Province-A (**Figure 1d**). Geochemically, the LP is depleted in K, Th, and H_2O relative to the AMC. LP follows the general K and Th crustal correlation on Mars and substantially overlaps with the K and Th distribution in Hesperia and Thaumasia Planum (**Figures 3e** and **S3**). Consequently, LP's K and Th depletion likely reflects volcanic resurfacing, not aqueous weathering (Taylor et al., 2006). H_2O depletion in the LP is also comparable in magnitude to that in the vicinity of Greater Thaumasia (Hood et al., 2016). Given minimal chemical weathering across the provinces (Section 4.1), the H_2O depletion is likely volcanic and could suggest a dry mantle source as predicted for Hesperian volcanism (cf., Balta & McSween, 2013). However, that mantle evolution model also predicts high Th abundances, not seen in our study. Overall, the LP likely follows the same volcanic evolution trends as identified in the Greater Thaumasia area, i.e., low H_2O abundance and temporally decreasing K and Th, maybe a part of the same evolving volcanic province (Hood et al., 2016). Furthermore, higher

K and Th abundance within LP relative to Greater Thaumasia could place it as the oldest member of an underlying volcanic series.

4.4. Medusae Fossae Formation (MFF) in Province-C

The discrete wind-sculpted outcrops of the mid-Noachian MFF extend along the martian equator (**Figure 1d**) and their origin remains uncertain (c.f., Kerber & Head, 2010; Zimbelman & Scheidt, 2012; Wilson et al., 2018). Geochemically, the MFF region is highly enriched in Fe, Ca, and volatiles (SO_3, Cl, and H_2O) relative to the AMC (**Figure S4**) (Keller et al., 2006). However, the abundance of K, Th, Al, Si, and the value of K/Th is consistent with the martian crust. As highly incompatible elements in igneous processes, the ratio of Cl/K would inherit the initial mantle abundance (Taylor et al., 2010). Although the ratio is globally maintained, the MFF region shows significantly different Cl/K than the rest of Mars. Chlorine is highly abundant, and K is generally lower than that in AMC (**Figures 3e** and **S4**), consistent with Cl enrichment in airborne dust and volcanic aerosol in the MFF (Newsom & Hagerty, 1997; Goetz et al., 2005). Meanwhile, high S and Cl content, moderately high H_2O (**Figure S5**), fine-grained nature, preserved primary mineralogy, and extensive erosional features suggest that MFF is the source of the global dust reservoirs of Mars (Ojha et al., 2018). Thus, our work supports the provenance of martian dust from mostly mechanical weathering and transport of a pyroclastic ashfall unit, which possibly arose from SW-oriented paleo-winds during Tharsis volcanic eruptions (Keller et al., 2006; Diez et al., 2009). Our results don't support the hypothesis of water-ice existence in polar layer-like deposits to explain the volatile enrichment in the equatorial MFF (Wilson et al., 2018). Summarily, the voluminous pyroclasts of MFF are most likely the product of low-moderate degree partial

melting of a distinct volatile-rich mantle source during mid-Noachian age in comparison to the late Noachian - Amazonian volcanic provinces of the martian highlands.

4.5. Southern Acidalia Planitia (SAP) in Province-D

SAP is a late Hesperian plain area (Tanaka et al., 2014) in the northern lowlands that geographically lies between Tharsis and Arabia Terra and is part of Province-D (**Figure 1d**). Geochemically, SAP is enriched in K, Th, Fe, Si and depleted in Al relative to the rest of the AMC (**Figure S6**). Despite K and Th enrichment, the K/Th ratio of SAP is consistent with the martian crust (**Figures 3e** and **S6**), which suggests primary rock composition (Karunatillake et al., 2006; Taylor et al., 2006), diverging from the extensive alteration posited by Bouley et al. (2020). Al/Si versus Mg/Si plots of SAP (**Figure S7a**) show a slope different from the martian crust but resembling that of younger martian meteorites (after, McSween et al., 2009). The Al depletion in SAP best correlates with that of the mean basaltic shergottite composition (Nimmo & Tanaka, 2005), and given the K, Th, and K/Th ratio signatures, it is more likely to be related to mantle composition than chemical weathering (Taylor et al., 2006) at least at the scales of our observations. Further, mineralogical observations by Compact Reconnaissance Imaging Spectrometer for Mars (CRISM) reveal mafic mineral signatures in outcrops, crater ejecta, and central peaks of the craters in SAP (Pan et al., 2017) resembling Hesperian-aged volcanism (Salvatore et al., 2010). Also, the non-detection of Al-bearing sulfates (**Figure S7b**) that would result from low-pH aqueous alteration (McLennan, 2012) supports an igneous origin for the apparent depletion of Al. The collective K and Th enrichment and Al-depletion can best be explained by a low degree of partial melting at high pressure derived from a garnet-rich mantle source for SAP.

5. Summary and Conclusion

The first consolidated chemical provinces of Mars reveal several geochemical signatures of broad geologic import. Our findings demonstrate secular chemical trends among the southern highland provinces A-C may indicate complex processes of an evolving degree of partial melting within a highly differentiated mantle source. Distinct lithology of the late Hesperian lowland unit, Province-D, does not follow the secular chemical trends like highland provinces. This could provide a mechanism for sampling a high-pressure, garnet-rich source for Province-D. We also find that even older volatile-rich regions preserve igneous geochemistry, indicating how throughout Mars's geologic history, water-limited isochemical weathering dominated regionally to decimeter depths scales. Specifically, as a distinct plateau of early Hesperian-aged highlands, the Lunae Planum region shows compositional links – and possibly shared provenance - with Province-A, much like Hesperia Planum, Syrtis Major, and part of Greater Thaumasia. The similarity of Province-C's K/Th trend with the average crust and enrichment of volatiles (especially S and Cl) supports mostly regional volcanic materials (e.g., ashfall pyroclastic deposits), especially for the Medusae Fossae Formation, despite volatiles' enrichment. In contrast to the provinces A-C, Southern Acidalia Planitia of Province-D in the northern lowlands is lithologically distinct with the highest abundance of K and Th of the provinces. However, the similarity of K/Th and depletion of Al relative to the average crust argues against sedimentary signatures of putative paleo-ocean(s). The northern lowlands may mostly represent the mafic crust of Mars, which might have originated by a low degree of partial melting at high pressure as suggested by high abundances of incompatible elements (K, Th) and Al- depletion rather than the conventional thought that the northern lowlands are highly fractionated. These findings also demonstrate the overall utility of the integrative multivariate methodology we have

developed for martian geochemical data, motivating possible applications to other planetary bodies (e.g., Mercury, Moon, and Vesta) with comparable datasets.

Acknowledgment

AR, ABS, and SN were supported by the Indian Space Research Organization, Director PRL, Head of Planetary Sciences Division, PRL, and Director IIT Gandhinagar. DRH is supported by the Baylor Office of the Vice Provost of Research Postdoctoral Program. OG's contribution was supported by the CNES, based on observations with GRS embarked on Odyssey. SK's participation was supported by NASA MDAP 80NSSC18K1375. The authors acknowledge anonymous reviewers for providing constructive and thorough reviews of the manuscript and Andrew Dombard for editorial handling.

Data Availability Statement: Data in support of this work can be found through Mendeley data (doi: 10.17632/3jd9whd78m.1). Archival GRS-derived chemical maps are from NASA Planetary Database System (PDS, https://pds-geosciences.wustl.edu/missions/odyssey/grs_cgs.html). Mars geology map taken from USGS-310 archive (https://pubs.usgs.gov/sim/3292/), and topographic data from MOLA-HRSC blended DEM data by Fergason et al. (2018).

Figure Caption

Figure 1: Results obtained from multivariate analysis by NHC-PCA **(a)**, HC-PCA **(b)**, and t-GTC **(c)** methods, overlaid on the Mars Orbiter Laser Altimeter and High-Resolution Stereo Camera (MOLA-HRSC) data map (Smith et al., 2001) to delineate the geochemical provinces. Provinces-2 and -4 do not appear in the t-GTC method **(c)** as they are compositionally similar to the average crustal composition (**Tables S2 and S3**). **(d)** The consolidated geochemical provinces on Mars are derived by integrating provinces from three different multivariate techniques and overlaid onto mapped geology (Tanaka et al., 2014;

different colors indicate different geologic units with major units in legend). The white dashed outline areas delineate our regional (LP, SAP, and MFF) case studies.

Figure 2: (a) The relative areal fractions of secular, transitional, and volcanic units within each chemical province corresponding to the consolidated geochemical map. The prefix "N" indicates Noachian, "H" indicates Hesperian, and "A" indicates Amazonian, and suffix "v" indicates the associated volcanic units (after, Tanaka et al., 2014). A detailed version of Figure 2a is given in Figure S2, both as per Tanaka et al. (2014) geology map. **(b)** Modified box-and-whiskers diagram to compare the distribution of elements for all provinces to the global geochemistry of the AMC. The top of the upper box represents 75^{th} percentile/25^{th} percentile ratio, the bottom of the lower box represents the $25^{th}/75^{th}$ percentile ratio, and the ratio of the medians by the boundary between them. The whiskers here represent the uncertainty on the ratio of medians using the Median Absolute Deviation (MAD) (Karunatillake et al., 2011). **(c)** The Chemical Index of Alteration ($CIA=100*[Al_2O_3/(Al_2O_3+CaO+Na_2O+K_2O)]$) diagram is used to assess the extent of chemical weathering in the provinces A-D. For CIA, we are using standard molar abundances of oxides. Non-GRS Na_2O is calculated using Baratoux et al. (2014).

Figure 3: Diagrams of K/Th normalized to the bulk silicate Mars (~ 5300) versus GRS derived total volatile concentration **(a)**, Fe versus Si **(b)**, Al versus Fe **(c)**, and Ca versus Si **(d)** of the provinces A-D are represented by colored boxes (southern highland provinces A-C) and ellipse (northern lowland Province-D). The modest variation in K/Th is consistent with the bulk Mars, implies to low or no alteration at decimeter depths in the consolidated provinces. The regional uncertainty is shown at the right corner of each plot, represented by

391 the average of standard error of mean (1σ) from all provinces (**Table 1**). From Noachian to
392 Amazonian, all the three plots **(b-d)** exhibit a compositional trend, marked by a dashed
393 arrow, except Province-D (**Figure S2**). The prefix "N" indicates Noachian, "H" indicates
394 Hesperian, and "A" indicates Amazonian, and the suffix "v" indicates associated volcanic
395 units, "h" indicates highland, "m" indicates middle and "lHl" indicates late Hesperian
396 lowland. **(e)** The scatter values of K (wt. %) versus Th (mg/kg) in Southern Acidalia Planitia
397 (SAP), Lunae Planum (LP), Medusae Fossae Formation (MFF), consolidated provinces A-D,
398 and AMC. SAP, LP, and MFF generally follow the same trend of K/Th as the AMC.
399
400
401
402
403
404
405
406
407
408
409
410
411

412 ## References

413 Balta, J. B., & McSween Jr, H. Y. (2013). Water and the composition of Martian magmas.
414 *Geology*, *41*, 1115-1118. https://doi.org/10.1130/G34714.1.

415 Bandfield, J. L., Hamilton, V. E., & Christensen, P. R. (2000). A global view of Martian
416 surface compositions from MGS-TES: *Science*, *287*, 1626-1630,
417 https://doi.org/10.1126/science.287.5458.1626.

418 Baratoux, D., Toplis, M. J., Monnereau, M., & Gasnault, O. (2011). Thermal history of Mars
419 inferred from orbital geochemistry of volcanic provinces. *Nature*, *472*, 338–341.
420 https://doi.org/10.1038/nature09903

421 Baratoux, D., Toplis, M. J., Monnereau, M., & Sautter, V. (2013). The petrological
422 expression of early Mars volcanism. *Journal of Geophysical Research: Planets*, *118(1)*,
423 59-64.https://doi.org/10.1029/2012JE004234

424 Baratoux, D., Samuel, H., Michaut, C., Toplis, M. J., Monnereau, M., Wieczorek, M., et al.
425 (2014). Petrological constraints on the density of the Martian crust. *Journal of*
426 *Geophysical Research: Planets*. *119*, 1707-1727.
427 https://doi.org/10.1002/2014JE004642

428 Basu Sarbadhikari, A., Babu, E. V. S. S. K., Vijaya Kumar, T., & Aoudjehane, H. C. (2016).
429 Martian meteorite Tissint records unique petrogenesis among the depleted shergottites.
430 *Meteoritics and Planetary Science*, *51*:1588–1610. https://doi.org/10.1111/maps.12684

431 Basu Sarbadhikari, A., Babu, E. V. S. S. K., & Vijaya Kumar, T. (2017). Chemical layering
432 in the upper mantle of Mars: Evidence from olivine-hosted melt inclusions in Tissint.
433 *Meteoritics and Planetary Science*, *52*, 251-267. https://doi.org/10.1111/maps.12790

434 Bevington, P. R., & Robinson, D. K. (2003). Data reduction and error analysis. *McGraw-Hill*,

New York.

Borg, L. E., & D. S. Draper (2003). A petrogenetic model for the origin and compositional variation of the Martian basaltic meteorites, *Meteoritics & Planetary Science*, 38, 1713–1731. https://doi.org/10.1111/j.1945-5100.2003.tb00011.x

Bouley, S., Keane, J.T., Baratoux, D., Langlais, B., Matsuyama, I., et al. (2020). A thick crustal block revealed by reconstructions of early Mars highlands. *Nature Geoscience*. 13, 105–109. https://doi.org/10.1038/s41561-019-0512-6

Boynton, W. V, Taylor, G. J., Evans, L. G., Reedy, R. C., Starr, R., Janes, D. M., et al. (2007). Concentration of H, Si, Cl, K, Fe, and Th in the low- and mid-latitude regions of Mars. *Journal of Geophysical Research: Planets*, *112*, 1–15, https://doi.org/10.1029/2007JE002887

Charrad M., Ghazzali N., Boiteau V., & Niknafs A. (2014). NbClust: An R Package for Determining the Relevant Number of Clusters in a Data Set. *Journal of Statistical Software*, 61, 1-36. http://www.jstatsoft.org/v61/i06/.

Cormack, R. M. (1971). A review of classification. *Journal of the Royal Statistical Society: Series A* (General), 134, 321-353.

Dasgupta, R., & Hirschmann, M.M. (2007). A modified iterative sandwich method for determination of near-solidus partial melt compositions. II. Application to determination of near-solidus melt compositions of carbonated peridotite, *Contributions to Mineralogy and Petrology, 154*, 647–661, https://doi.org/10.1007/s00410-007-0214-8.

Diez, B., Feldman, W. C., Maurice, S., Gasnault, O., Prettyman, T. H., & Mellon, M. T. (2008). H layering in the top meter of Mars. *Icarus*, *196*, 409–421. https://doi.org/10.1016/j.icarus.2008.02.006

459 Diez, B., Feldman, W. C., Mangold, N., Baratoux, D., Maurice, S., Gasnault, O., et al.
460 (2009). Contribution of mars odyssey GRS at central elysium planitia. *Icarus*, *2001*, 19-
461 29. https://doi.org/10.1016/j.icarus.2008.11.011

462 Ehlmann, B. L., Mustard, J. F., Murchie, S. L., Bibring, J. P., Meunier, A., Fraeman, A. A., &
463 Langevin, Y. (2011). Subsurface water and clay mineral formation during the early
464 history of Mars. *Nature*, *479*, 53–60. https://doi.org/10.1038/nature10582

465 Feldman, W. C., Head, J. W., Maurice, S., Prettyman, T. H., Elphic, R. C., Funsten, H. O., et
466 al. (2004). Recharge mechanism of near-equatorial hydrogen on Mars: Atmospheric
467 redistribution or sub-surface aquifer. *Geophysical Research Letters*, *31*, 2–5.
468 https://doi.org/10.1029/2004GL020661

469 Feldman, W. C., Pathare, A., Maurice, S., Prettyman, T. H., Lawrence, D. J., Milliken, R. E.,
470 & Travis, B. J. (2011). Mars Odyssey neutron data: 2. Search for buried excess water
471 ice deposits at nonpolar latitudes on Mars. *Journal of Geophysical Research: Planets*,
472 *116*, E11009. https://doi.org/10.1029/2011JE003806

473 Fergason, R. L., Hare, T. M., & Laura, J. (2018). HRSC and MOLA blended digital elevation
474 Model at 200m v2. *Astrogeology PDS annex. U.S. Geological Survey*. Retrieved from
475 http://bit.ly/HRSC_MOLA_Blend_v0.

476 Gasnault, O., Taylor, J. G., Karunatillake, S., Dohm, J., Newsom, H., Forni, O., et al. (2010).
477 Quantitative geochemical mapping of martian elemental provinces. *Icarus*, *207*, 226–
478 247. https://doi.org/10.1016/j.icarus.2009.11.010

479 Goetz, W., Bertelsen, P., Binau, C. S., Gunnlaugsson, H. P., Hviid, S. F., Kinch, K. M., et al.
480 (2005). Indication of drier periods on Mars from the chemistry and mineralogy of
481 atmospheric dust. *Nature. 436*, 62–65. https://doi.org/10.1038/nature03807

Golombek, M.P., & Phillips, R.J. (2009) Mars tectonics, *Planetary tectonics*. *Cambridge University Press*, 11, 180–232.

Grott, M., Baratoux, D., Hauber, E., Sautter, V., Mustard, J., Gasnault, O., et al. (2013). Long-term evolution of the Martian crust-mantle system, *Space Science Reviews*, *174(1)*, 49-111. https://doi.org/10.1007/s11214-012-9948-3

Halevy, I., Zuber, M. T., & Schrag, D. P. (2007). A Sulfur Dioxide Climate Feedback on Early Mars, *Science*, *318*, 1903–1908. https://doi.org/10.5040/9780755621101.0007

Hood, D. R., Judice, T., Karunatillake, S., Rogers, D., Dohm, J. M., Susko, D., & Carnes, L. K. (2016). Assessing the geologic evolution of Greater Thaumasia, Mars. *Journal of Geophysical Research: Planets*. *121*, 1753–1769, https://doi.org/10.1002/2016JE005046

Hood, D. R., Karunatillake, S., Gasnault, O., Williams, A. J., Dutrow, B., Ojha, L., Kobs, S., Kim, K., Heldmann, J., & Fralick, C. (2019). Contrasting regional soil alteration across the topographic dichotomy of Mars. *Geophysical Research Letters*, *46*, 13668-13677. https://doi.org/10.1029/2019GL084483

Hurowitz, J. A., & McLennan, S. M. (2007). A ~3.5 Ga record of water-limited, acidic weathering conditions on Mars, *Earth and Planetary Science Letters*, 260 (3–4), 432–443, https://doi.org/10.1016/j.epsl.2007.05.043.

Karunatillake, S., Squyres, S. W., Taylor, G. J., Keller, J. M., Gasnault, O., Evans, L. G., et al. (2006). Composition of northern low-albedo regions of Mars: Insights from the Mars Odyssey Gamma Ray Spectrometer. *Journal of Geophysical Research*, *111*. https://doi.org/10.1029/2006JE002675

504 Karunatillake, S., Wray, J. J., Squyres, S. W., Taylor, G. J., Gasnault, O., Mclennan, S. M., et
505 al. (2009). Chemically striking regions on Mars and Stealth revisited, *Journal of*
506 *Geophysical Research: Planets*, *114*, 1–35. https://doi.org/10.1029/2008JE003303

507 Karunatillake, S., Squyres, S. W., Gasnault, O., Keller, J. M., Janes, D. M., Boynton, W. V.,
508 et al. (2011). Recipes for spatial statistics with global datasets: a martian case study.
509 *Journal of Scientific Computing, 46*, 439-451. https://doi.org/10.1007/s10915-010-
510 9412-z

511 Kaufman, L., & Rousseeuw, P.J. (2005). Finding Groups in Data: An Introduction to Cluster
512 Analysis. *John Wiley & Sons*, New York.

513 Keller, J. M., Boynton, W. V, Karunatillake, S., Baker, V. R., Dohm, J. M., Evans, L. G., et
514 al. (2006). Equatorial and midlatitude distribution of chlorine measured by Mars
515 Odyssey GRS. *Journal of Geophysical Research: Planets*, *111*, 1–18.
516 https://doi.org/10.1029/2006JE002679

517 Kerber, L., & Head, J. W. (2010). The age of the Medusae Fossae Formation: Evidence of
518 Hesperian emplacement from crater morphology, stratigraphy, and ancient lava
519 contacts. *Icarus*, *206* (2), 669–684. https://doi.org/10.1016/j.icarus.2009.10.001

520 King, P.L., & McLennan, S.M. (2010). Sulfur on Mars. Elements 6, 107-112.

521 Maurice, S., Feldman, W., Diez, B., Gasnault, O., Lawrence, D. J., Pathare, A., & Prettyman,
522 T. (2011). Mars Odyssey neutron data: 1. Data processing and models of water-
523 equivalent-hydrogen distribution. *Journal of Geophysical Research: Planets*, *116*.
524 https://doi.org/10.1029/2011JE003810

525 McLennan, S. M. (2012). Geochemistry of Sedimentary Processes on Mars, Sedimentary
526 Geology of Mars. *Sedimentary Geology of Mars*. Special Publication *102*, 119–138,
527 https://doi.org/10.2110/pec.12.102.0119

McSween Jr, H. Y., Taylor, G. J., & Wyatt, M. B. (2009). Elemental Composition of the Martian Crust. *Science, 324(5928), 736-739*. https://doi.org/10.1126/science.1165871

Newsom, H. E., & Hagerty, J. J. (1997). Chemical components of the Martian soil: Melt degassing, hydrothermal alteration, and chondritic debris. *Journal of Geophysical Research: Planets*, *102*, 19345-19355. https://doi.org/10.1029/97JE01687

Nimmo, F., & Tanaka, K. (2005). Early crustal evolution of Mars. *Annual Review of Earth and Planetary Sciences*, *33*, 133–161. https://doi.org/10.1146/annurev.earth.33.092203.122637

Ojha, L., Lewis, K., Karunatillake, S., & Schmidt, M. (2018). The Medusae Fossae Formation as the single largest source of dust on Mars. *Nature Communications*, *9*, 1–7. https://doi.org/10.1038/s41467-018-05291-5

Ojha, L., Karunatillake, S., Karimi, S., & Buffo, J. (2021). Amagmatic hydrothermal systems on Mars from radiogenic heat. *Nature Communications*, *12*, 1-11. https://doi.org/10.1038/s41467-021-21762-8

Pan, L., Ehlmann, B. L., Carter, J., & Ernst, C. M. (2017). The stratigraphy and history of Mars' northern lowlands through mineralogy of impact craters. A comprehensive survey. *Journal of Geophysical Research: Planets*, *122*, 1824–1854. https://doi.org/10.1002/2017JE005276

Plesa, A.C., Padovan, S., Tosi, N., Breuer, D., Grott, M., Wieczorek, M. A., et al. (2018). The thermal state and interior structure of Mars. *Geophysical Research Letters*, *45*, 198–12. https://doi.org/10.1029/2018GL080728

549 Rogers, A. D., Bandfield, J. L., & Christensen, P. R. (2007). Global spectral classification of
550 Martian low-albedo regions with Mars Global Surveyor Thermal Emission
551 Spectrometer (MGS-TES) data. *112*, 1–29. https://doi.org/10.1029/2006JE002726

552 Rogers, A. D., & Hamilton, V. E. (2015). Compositional provinces of Mars from statistical
553 analyses of TES, GRS, OMEGA and CRISM data. *Journal of Geophysical Research:*
554 *Planets*, *120*, 62–91. https://doi.org/10.1002/2014JE004690

555 Rousseeuw, P.J. (1987). Silhouettes: A graphical aid to the interpretation and validation of
556 cluster analysis. *Journal of Computational and Applied Mathematics*, 20, 53–65.

557 Salvatore, M. R., Mustard, J. F., Wyatt, M. B., & Murchie, S. L. (2010). Definitive evidence
558 of Hesperian basalt in Acidalia and Chryse Planitiae. *Journal of Geophysical Research*,
559 *115*, E07005. https://doi.org/10.1029/2009JE003519

560 Smith, D. E., Zuber, M. T., Frey, H. V., Garvin, J. B., Head, J. W., Muhleman, D. O., et al.
561 (2001). Mars Orbiter Laser Altimeter: Experiment summary after the first year of
562 global mapping of Mars. *Journal of Geophysical Research: Planets*, *106*, 23689-23722.
563 https://doi.org/10.1029/2000JE001364

564 Tanaka, K. L., Skinner, J. A., Dohm, J. M., Irwin, R. P., I., Kolb, E. J., Fortezzo, C. M., et al.
565 (2014). Description of Map Units, p. 1–43, https://doi.org/10.133/sim3292

566 Taylor, G. J. (2013). The bulk composition of Mars. *Geochemistry*. 73, 401-420.
567 https://doi.org/10.1016/j.chemer.2013.09.006

568 Taylor, G. J., Stopar, J. D., Boynton, W. V., Karunatillake, S., Keller, J. M., Brückner, J., et
569 al. (2006). Variations in K/Th on Mars. *Journal of Geophysical Research*, *112*,
570 E03S06. https://doi.org/10.1029/2006JE002676

571 Taylor, G. J., Martel, L. M. V., Karunatillake, S., Gasnault, O., & Boynton, W. V. (2010).
572 Mapping Mars geochemically. *Geology*, *38*, 183–186.
573 https://doi.org/10.1130/G30470.1

574 Tosca, N. J., McLennan, S. M., Dyar, M. D., Sklute, E. C., & Michel, F. M. (2008). Fe
575 oxidation processes at Meridiani Planum and implications for secondary Fe mineralogy
576 on Mars. *Journal of Geophysical Research: Planets*, 113(E5).
577 https://doi.org/10.1029/2007JE003019

578 Treiman, A.H., (2005). The nakhlite meteorites: Augite-rich igneous rocks from Mars:
579 *Chemie der Erde Geochemistry*, *65*, 203–270,
580 https://doi.org/10.1016/j.chemer.2005.01.004.

581 Udry, A., Howarth, G. H., Herd, C. D. K., Day, J. M., Lapen, T. J., & Filiberto, J. (2020).
582 What martian meteorites reveal about the interior and surface of Mars, *Earth Space*
583 *Science Open Archive 55*, https://doi.org/10.1002/essoar.10503123.1.

584 Wilson, J. T., Eke, V. R., Massey, R. J., Elphic, R. C., Feldman, W. C., Maurice, S., &
585 Teodoro, L. F. A. (2018). Equatorial locations of water on Mars: Improved resolution
586 maps based on Mars Odyssey Neutron Spectrometer data. *Icarus*, 299, 148–160.
587 https://doi.org/10.1016/j.icarus.2017.07.028

588 Zimbelman, J. R., & Scheidt, S. P. (2012). Hesperian Age for Western Medusae, Mars,
589 *Science*, *336*(6089), 1683-1683. https://doi.org/10.1126/science.1221094

590

Figure 1.

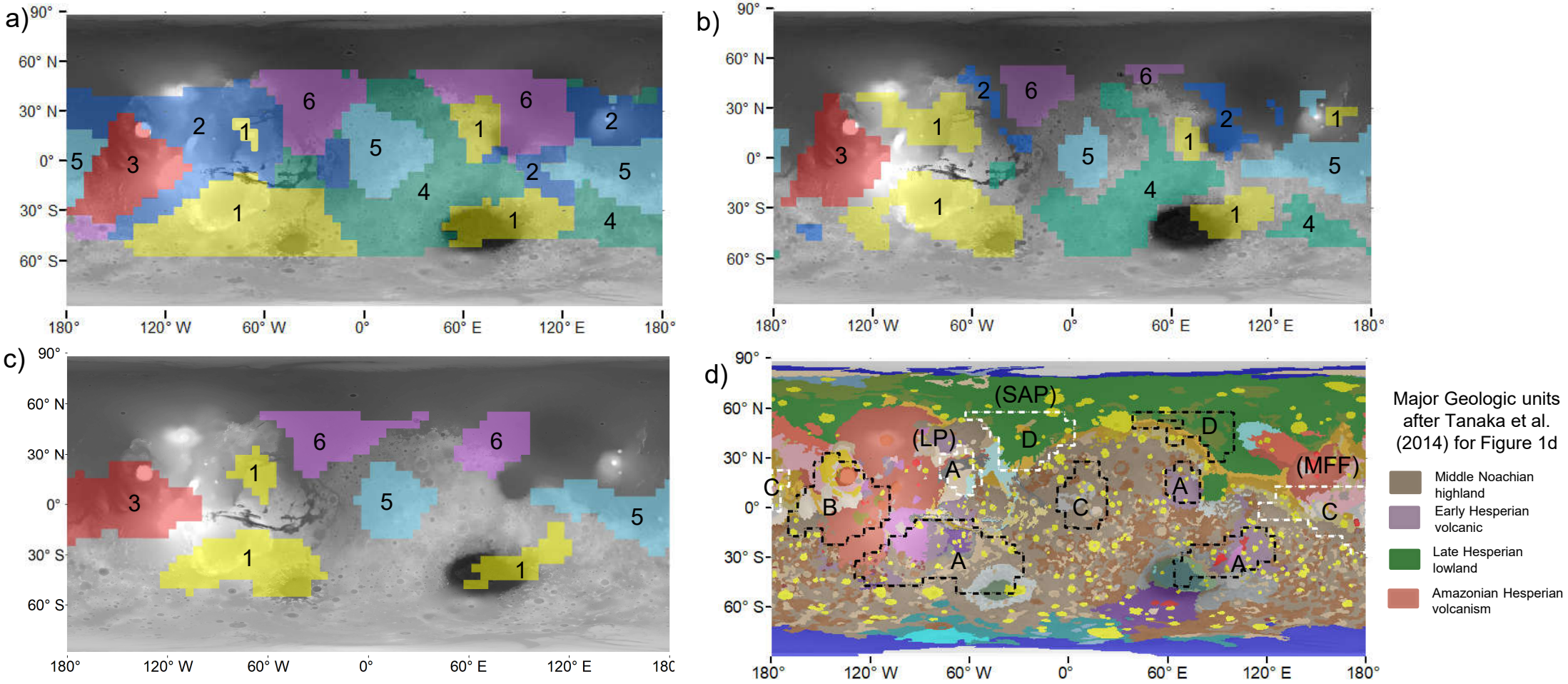
a)
b)
c)
d)
90°
60° N
30° N
0°
30° S
60° S
180°
120° W
60° W
0°
60° E
120° E
180°
(SAP)
(LP)
(MFF)
A
B
C
D
Major Geologic units after Tanaka et al. (2014) for Figure 1d
Middle Noachian highland
Early Hesperian volcanic
Late Hesperian lowland
Amazonian Hesperian volcanism

Figure 2.

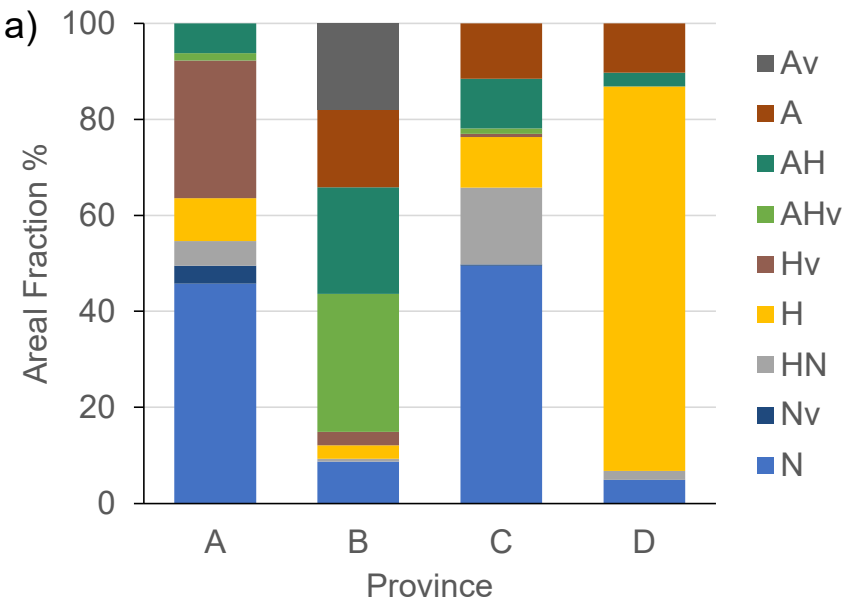
a)
100
80
60
40
20
0
Areal Fraction %
A
B
C
D
Province
Av
A
AH
AHv
Hv
H
HN
Nv
N

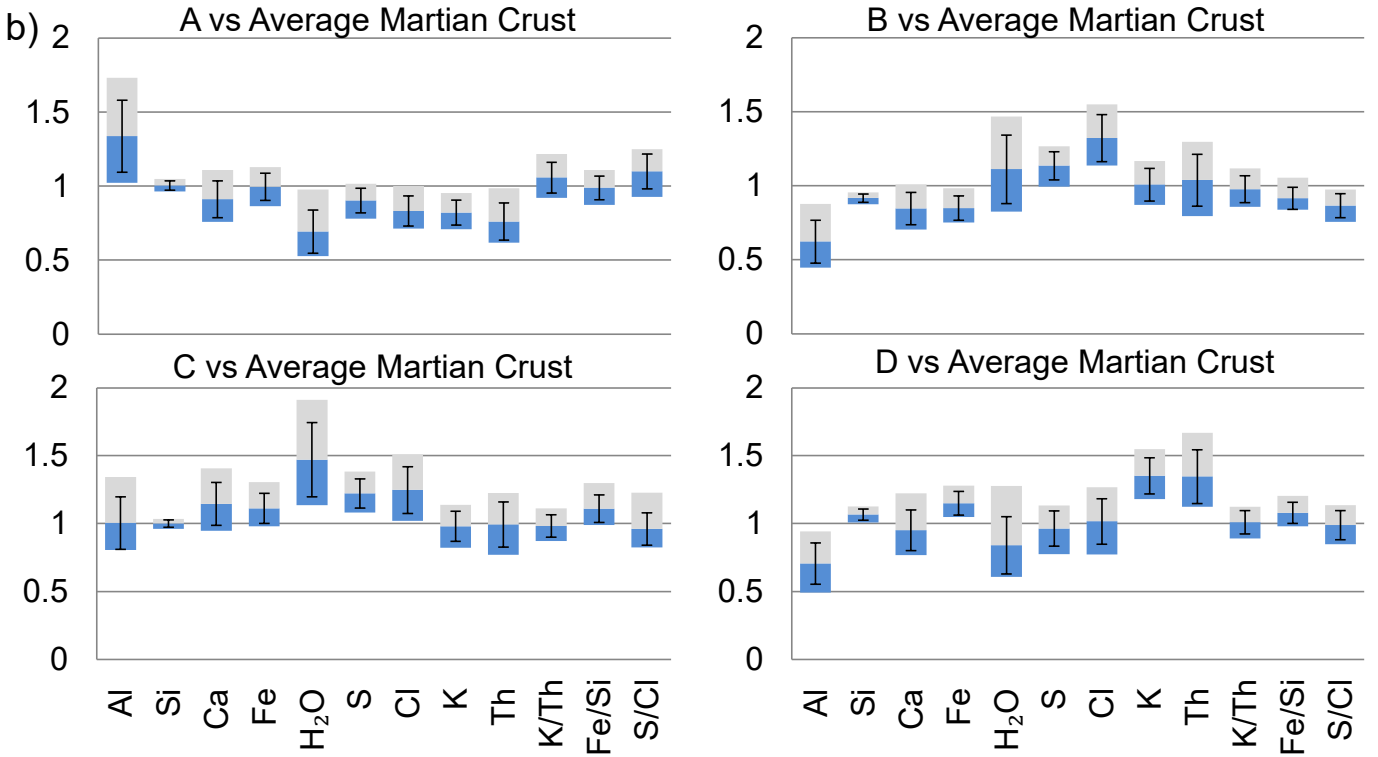
b)
A vs Average Martian Crust
B vs Average Martian Crust
C vs Average Martian Crust
D vs Average Martian Crust
2
1.5
1
0.5
0
Al
Si
Ca
Fe
H2O
S
Cl
K
Th
K/Th
Fe/Si
S/Cl

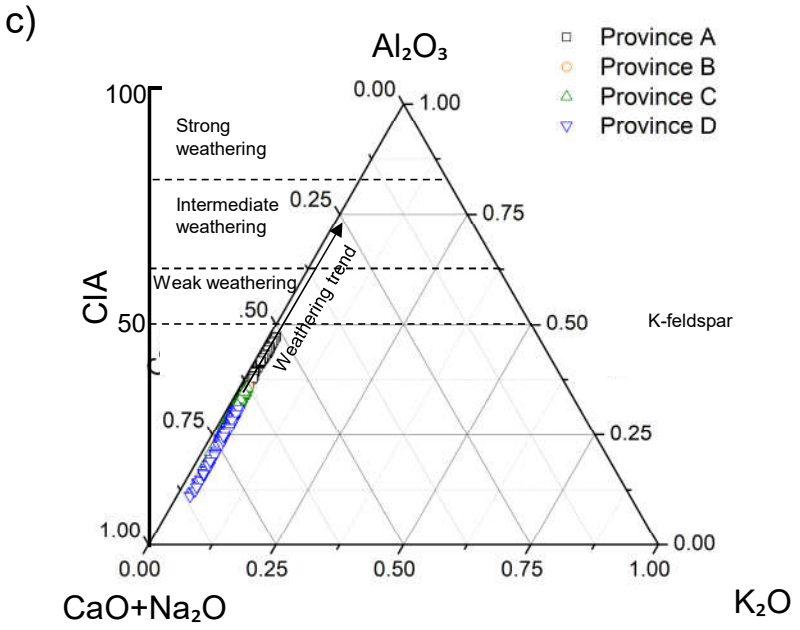
c)
Al2O3
CaO+Na2O
K2O
Province A
Province B
Province C
Province D
Strong weathering
Intermediate weathering
Weak weathering
Weathering trend
K-feldspar
CIA
100
50
0.00
0.25
0.50
0.75
1.00

Figure 3.

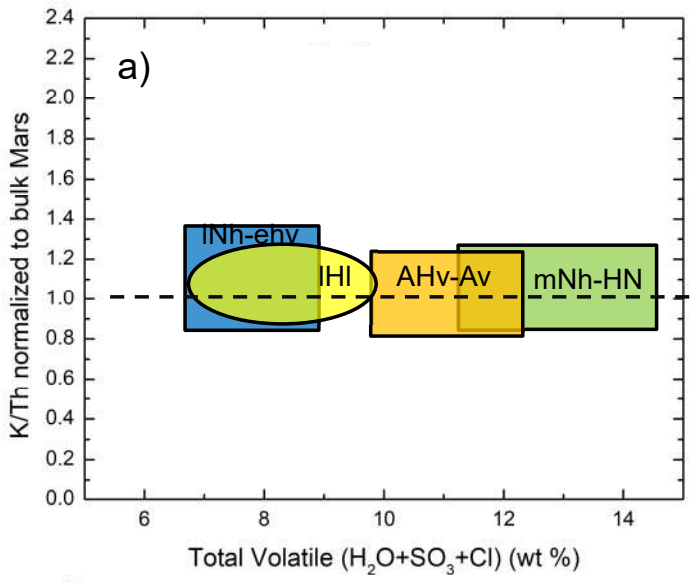
a)
K/Th normalized to bulk Mars
Total Volatile (H2O+SO3+Cl) (wt %)
lNh-ehv
lHl
AHv-Av
mNh-HN

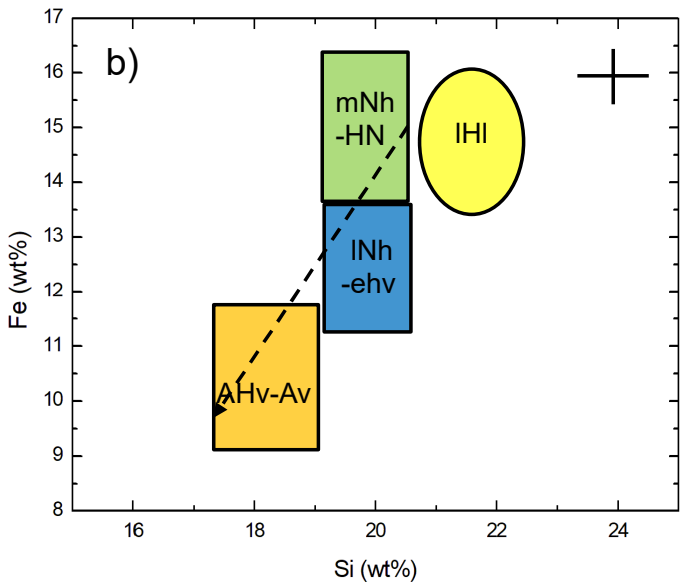
b)
Fe (wt%)
Si (wt%)
mNh
-HN
lHl
lNh
-ehv
AHv-Av

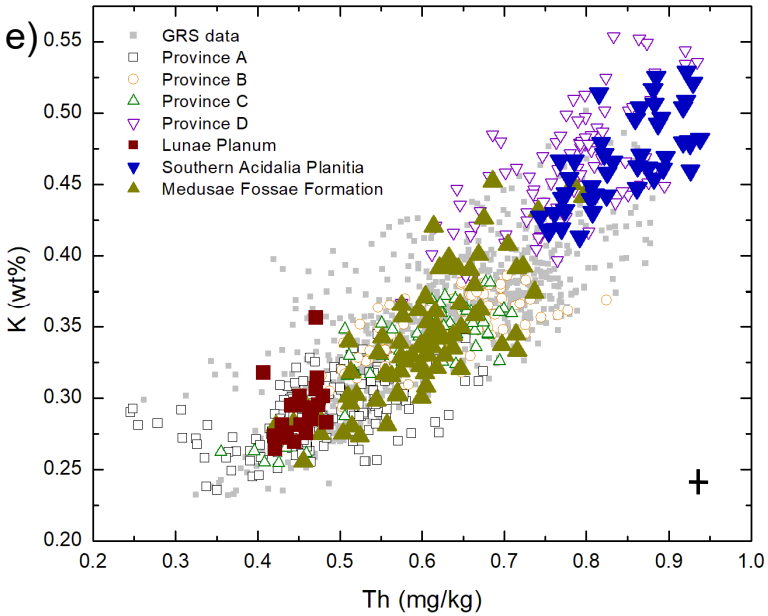
e)
K (wt%)
Th (mg/kg)
GRS data
Province A
Province B
Province C
Province D
Lunae Planum
Southern Acidalia Planitia
Medusae Fossae Formation

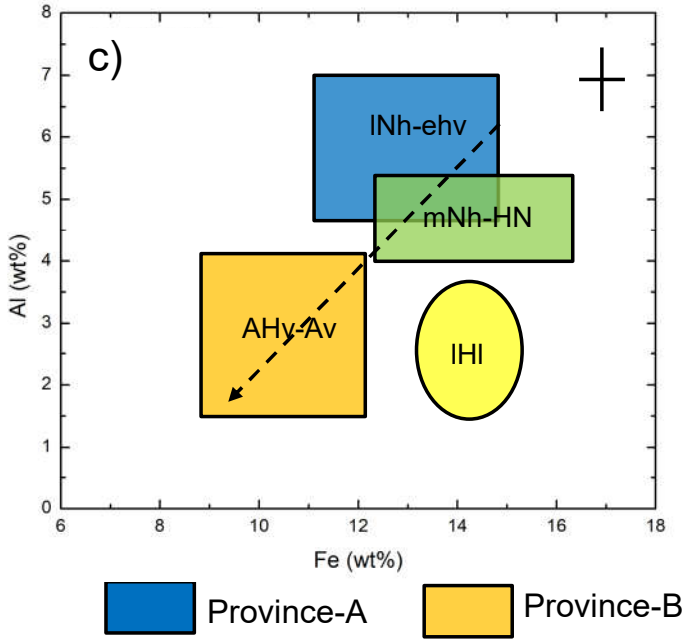
c)
Al (wt%)
Fe (wt%)
lNh-ehv
mNh-HN
AHv-Av
lHl

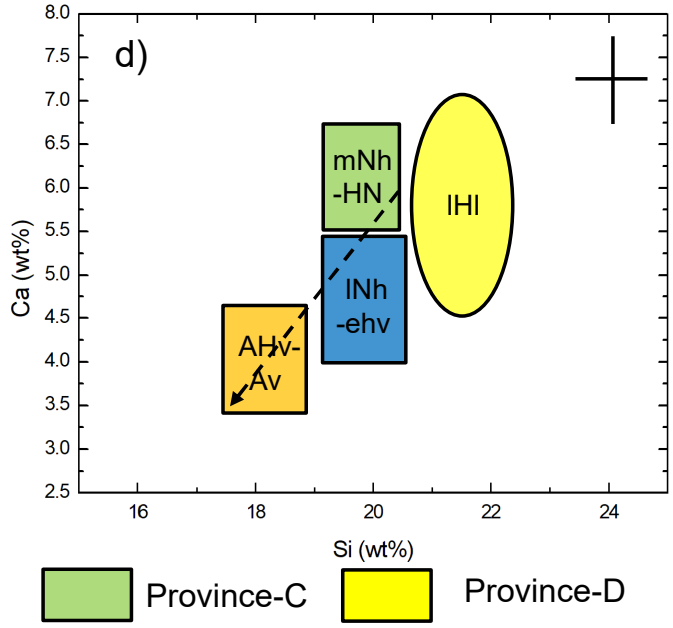
d)
Ca (wt%)
Si (wt%)
mNh
-HN
lHl
lNh
-ehv
AHv-
Av

Province-A
Province-B
Province-C
Province-D

Table 1: Arithmetic mean stoichiometric oxide mass fraction as a percentage (wt%, if not mentioned otherwise), elemental ratio, and its corresponding root means square uncertainty (σ) are calculated from mean measurement uncertainties for the grid points composing a geochemical province. Whereas, K/Th ratio uncertainty is calculated from $[(K/Th)*((\sigma_K/K)^2+((\sigma_{Th}/Th)^2]^{1/2}$ (GRS derived) of the consolidated chemical provinces.

	Province-A	**Province-B**	**Province-C**	**Province-D**	**Mid-latitudinal Average Martian Crust (AMC)**
K_2O	0.35±0.01	0.42±0.01	0.40±0.01	0.56±0.02	0.43±0.01
FeO	16.1±0.9	14.0±0.8	18.2±1.1	18.4±1.2	16.3±1.0
SiO_2	42.7±2.3	39.1±2.1	42.4±2.6	44.9±3.0	42.5±2.5
CaO	6.6±1.2	5.9±1.1	7.9±1.4	6.9±1.7	7.0±1.3
Th mg/kg	0.48±0.04	0.62±0.05	0.59±0.05	0.80±0.06	0.61±0.05
Al_2O_3	10.6±2.1	5.5±1.8	8.6±2.2	6.2±2.6	8.5±2.2
H_2O	2.9±0.4	4.2±0.4	5.5±0.5	3.5±0.6	3.9±0.5
Cl	0.41±0.03	0.61±0.03	0.57±0.04	0.46±0.04	0.47±0.03
SO_3	4.9±0.5	6.0±0.5	6.5±0.6	5.2±0.7	5.4±0.6
K/Th	6060±580	5600±430	5680±520	5800±440	5760±470